# Searching for axionlike dark matter by amplifying a weak magnetic field with the quantum Zeno effect

Jing Dong,[1,2,3,4] W. T. He,[5] S.-D. Zou,[1] D. L. Zhou,[2,3] and Qing Ai[1,4,*]

[1]*School of Physics and Astronomy, Applied Optics Beijing Area Major Laboratory, Beijing Normal University, Beijing 100875, China*

[2]*Institute of Physics, Chinese Academy of Sciences, Beijing 100190, China*

[3]*University of Chinese Academy of Sciences, Beijing 100049, China*

[4]*Key Laboratory of Multiscale Spin Physics, Ministry of Education, Beijing Normal University, Beijing, China*

[5]*Quantum Dynamics Unit, Okinawa Institute of Science and Technology, Tancha 1919-1, Okinawa 904-0495, Japan*

(Received 19 February 2025; accepted 27 October 2025; published 17 November 2025)

The enhancement of weak signals and the detection of hypothetical particles facilitated by quantum amplification are crucial for advancing fundamental physics and its practical applications. Recently, it was experimentally observed that a magnetic field can be amplified by using nuclear spins under Markovian noise [H. Su *et al.*, New constraints on axion-mediated spin interactions using magnetic amplification, Phys. Rev. Lett. **133**, 191801 (2024).]. Here, we theoretically propose amplifying the magnetic-field signal by using nuclear spins by the quantum Zeno effect (QZE). Under identical conditions, we demonstrate that compared to the Markovian case the amplification of the weak magnetic field can be enhanced by a factor about $e^{1/2}$ under a Gaussian noise. Moreover, through numerical simulations we determine the optimal experimental parameters for amplification conditions. This work shows that the combination of the QZE and spin amplification effectively enhances the amplification of the weak magnetic field. Our findings may provide valuable guidance for the design of experiments on establishing new constraints of dark matter and exotic interactions in the near future.

DOI: 10.1103/nrww-mbk1

## I. INTRODUCTION

According to astrophysical observations, roughly five sixths of the matter in the Universe remains dark [1]. However, direct detection of its interactions with particles and fields of the standard model remains elusive [2]. There are a variety of particle candidates for dark matter, such as quantum chromodynamics axion and axionlike particles (ALPs) [3], new $Z'$ bosons [4], new spin-1 bosons [5], and dark photons [6,7]. Axions are prominent dark-matter and dark-energy candidates, which are introduced as a compelling solution to the strong-$CP$ problem beyond the standard model. However, it is insufficient to search for ALPs by traditional particle-physics techniques with light quanta such as the Large Hadron Collider [8,9]. Therefore, experimental searches for axionlike dark matter are based on their nongravitational interactions with particles and fields of the standard model [8–15].

As known to all, quantum amplification plays an important role in quantum metrology and finds applications in the measurements of weak field and force [16–19], and optical amplification [20] to search for new physics beyond the standard model [10]. Besides, the magnetic-field amplification finds applications in a wide range of searching axion-nucleon interactions, such as ALPs and axion bursts from astrophysical events [21,22]. Under state-of-the-art experiments, the sensitivity has exceeded astrophysical limits [23] by several orders of magnitude. We note that both electron and nuclear spins have shown great potential for realizing signal amplification. For example, the overlapping spin ensemble, e.g., $^{129}$Xe-$^{87}$Rb, is used in self-compensating comagnetometers [24–26]. Recently, magnetic-field amplification using $^{129}$Xe noble gas overlapped with spin-polarized $^{87}$Rb atomic gas was demonstrated, which has achieved a significant improvement in amplification of weak-field measurements under the Markovian noise, i.e., a constant spin relaxation rate [27].

On the other hand, the quantum Zeno effect (QZE) describes the phenomenon that a quantum system's dynamic evolution drastically slows down when measured frequently enough [28–33]. The QZE plays a vital role in various domains of quantum science. One of the applications of the QZE is quantum measurements, which can suppress the detrimental effects of decoherence [34,35]. By performing

*Contact author: aiqing@bnu.edu.cn

 

frequent error-correction measurements, the QZE helps stabilize the quantum state of qubits, thereby prolonging their coherence time and enhancing the reliability of quantum computations. Both theoretically and experimentally, it has been demonstrated that the QZE can enhance the quantum metrology by using the maximum-entangled states [36–38]. So far, the QZE has been experimentally observed in a number of physical systems such as trapped ions [39,40], ultracold atoms [41–43], molecules [44], Bose-Einstein condensates [45], nitrogen-vacancy centers [46], and superconducting quantum circuits [47–50].

To achieve the more significant amplification of external magnetic fields, in this paper, we propose a magnetic-field amplification using noble gas overlapped with spin-polarized alkali-metal gas by the QZE, which can achieve an improvement in the amplification of weak-field measurements as compared to the Markovian case. In weak magnetic fields, we obtain the analytical solution to the dynamics of $^{129}$Xe spins and amplification function, which present an enhancement of $e^{1/2}$ compared to the Markovian case. In the case of strong magnetic fields, we further examine the response of the $^{129}$Xe spins by numerical simulations under various conditions. Then, we provide the optimal measurement parameters for the practical experiments, i.e., the detuning between the Larmor frequency and the frequency of the magnetic field, the decoherence time, and the magnitude of the magnetic field. We anticipate that the present amplification technique could stimulate possible applications in applied and fundamental physics.

The rest of the paper is organized as follows: The model is set up and the response of polarized $^{129}$Xe spins to a transverse oscillating magnetic field is derived in Sec. II. Then, the response of polarized $^{129}$Xe spins in the case of weak magnetic fields is investigated in Sec. III. In Sec. IV, the transverse polarization of the polarized $^{129}$Xe spins is studied and the optimal amplification is explored in the case of strong magnetic fields. A summary is provided in Sec. V. Non-Markovian open quantum dynamics is derived in Appendix A. In Appendix B, we discuss how to prolong the transverse relaxation time.

## II. MODEL

According to Ref. [51], there are two cells containing nuclear spins, i.e., the source and the sensor cells. In order to tune the noble-gas Larmor frequency $\nu_0 = \gamma_n B_0/2\pi$ to match the oscillation frequency of the external transverse field $\mathbf{B}_{\rm ac}$, a bias magnetic field with strength $B_0$ is applied along the $z$-axis. Here, $\gamma_n$ is the gyromagnetic ratio of $^{129}$Xe. Due to the axion-mediated interaction between polarized neutrons, the $^{129}$Xe nuclear spins are also subject to a time-dependent transverse magnetic field. As a result, the $^{129}$Xe nuclear spin in a magnetic field is described by the following Hamiltonian:

$$\hat{H} = -\gamma_n \mathbf{B}(t)\cdot\hat{\mathbf{I}}, \tag{1}$$

where $\mathbf{B}(t) = B_0\hat{z} + B_{\rm ac}\cos(2\pi\nu t)\hat{y}$ is the total field experienced by $^{129}$Xe nuclear spins with $\nu$ being the Larmor frequency of the nuclear spins in the source cell, and $\gamma_n = 2\pi \times 11.78$ Hz/μT [27] and $\hat{\mathbf{I}} = (\hat{I}_x, \hat{I}_y, \hat{I}_z)$ are the gyromagnetic ratio and the angular momentum operators of $^{129}$Xe, respectively. The spin Hamiltonian with the total field reads explicitly

$$\hat{H} = -\gamma_n B_0 \hat{I}_z - \gamma_n B_{\rm ac}\cos(2\pi\nu t)\hat{I}_y. \tag{2}$$

According to the Heisenberg equation of motion, we can obtain the dynamical equation for the nuclear spin angular momentum as

$$\frac{d\hat{I}_x}{dt} = \gamma_n B_0 \hat{I}_y - \gamma_n B_{\rm ac}\cos(2\pi\nu t)\hat{I}_z, \tag{3}$$

$$\frac{d\hat{I}_y}{dt} = -\gamma_n B_0 \hat{I}_x, \tag{4}$$

$$\frac{d\hat{I}_z}{dt} = \gamma_n B_{\rm ac}\cos(2\pi\nu t)\hat{I}_x. \tag{5}$$

The polarization of $^{129}$Xe atoms can be defined as

$$\mathbf{P} = \frac{\langle\hat{\mathbf{I}}\rangle}{v_0}, \tag{6}$$

where $v_0^{-1}$ is the atomic number density. The dynamics of the three polarization components can be described by the Bloch equations as [52]

$$\frac{dP_x}{dt} = \gamma_n B_0 P_y - \gamma_n B_{\rm ac}\cos(2\pi\nu t)P_z, \tag{7}$$

$$\frac{dP_y}{dt} = -\gamma_n B_0 P_x, \tag{8}$$

$$\frac{dP_z}{dt} = \gamma_n B_{\rm ac}\cos(2\pi\nu t)P_x. \tag{9}$$

Generally speaking, any quantum system inevitably suffers from interaction with its environment. On account of a Markovian noise, the dynamics of $^{129}$Xe spins can be described with the Bloch equations

$$\frac{dP_x}{dt} = \gamma_n B_0 P_y - \gamma_n B_{\rm ac}\cos(2\pi\nu t)P_z - \frac{1}{T_2}P_x, \tag{10}$$

$$\frac{dP_y}{dt} = -\gamma_n B_0 P_x - \frac{1}{T_2}P_y, \tag{11}$$

$$\frac{dP_z}{dt} = \gamma_n B_{\rm ac}\cos(2\pi\nu t)P_x - \frac{1}{T_1}P_z, \tag{12}$$

where $T_1$ ($T_2$) is the longitudinal (transverse) relaxation time of the $^{129}$Xe spin. We consider the response of polarized $^{129}$Xe spins to a transverse oscillating magnetic field. Considering a Gaussian noise here, the dynamics of $^{129}$Xe spins can be described by the Bloch equation as [53]

$$\frac{dP_x}{dt} = \gamma_n B_0 P_y - \gamma_n B_{\rm ac}\cos(2\pi\nu t) P_z - \frac{t}{T_2^2} P_x, \quad (13)$$

$$\frac{dP_y}{dt} = -\gamma_n B_0 P_x - \frac{t}{T_2^2} P_y, \quad (14)$$

$$\frac{dP_z}{dt} = \gamma_n B_{\rm ac}\cos(2\pi\nu t) P_x - \frac{t}{T_1^2} P_z. \quad (15)$$

To analyze the system more conveniently, we transform it to the rotating frame defined by

$$\hat{U} = e^{i2\pi\nu\hat{I}_z}. \quad (16)$$

In the rotating frame, the effective Hamiltonian

$$\hat{\tilde{H}} = \hat{U}^\dagger \hat{H}\, \hat{U} - i\hat{U}^\dagger \frac{d}{dt}\hat{U} \quad (17)$$

can be simplified as

$$\hat{\tilde{H}} \approx \Delta \hat{I}_z - \frac{1}{2}\gamma_n B_{\rm ac}\hat{I}_y, \quad (18)$$

where $\Delta = 2\pi(\nu - \nu_0)$ is the detuning, and we have dropped the fast-oscillating terms by the rotating-wave approximation [31,53]. Thus, the Bloch equations of $^{129}$Xe spins in the rotating frame read

$$\dot{\tilde{P}}_x = \frac{\gamma_n B_{\rm ac}}{2}\tilde{P}_z + \Delta\tilde{P}_y - \frac{t}{T_2^2}\tilde{P}_x, \quad (19)$$

$$\dot{\tilde{P}}_y = -\Delta\tilde{P}_x - \frac{t}{T_2^2}\tilde{P}_y, \quad (20)$$

$$\dot{\tilde{P}}_z = -\frac{\gamma_n B_{\rm ac}}{2}\tilde{P}_x - \frac{t}{T_1^2}\tilde{P}_z, \quad (21)$$

where $\tilde{P}_\alpha(\alpha = x, y, z)$ are the polarizations of $^{129}$Xe spins in the rotating frame. Now, we can define the effective magnetic field in the rotating frame as $\tilde{\mathbf{B}} = (B_{\rm ac}/2)\hat{y} - (\Delta/\gamma_n)\hat{z}$.

When the Rb pump light is off, the effective magnetic-field gradient induced by the Rb polarization is greatly suppressed, resulting in $T_2$ being close to $T_1$ [51]. As a result, we assume $T_2 \approx T_1 = T$ and thus we have

$$\dot{\tilde{P}}_x = \frac{\gamma_n B_{\rm ac}}{2}\tilde{P}_z + \Delta\tilde{P}_y - \frac{t}{T^2}\tilde{P}_x, \quad (22)$$

$$\dot{\tilde{P}}_y = -\Delta\tilde{P}_x - \frac{t}{T^2}\tilde{P}_y, \quad (23)$$

$$\dot{\tilde{P}}_z = -\frac{\gamma_n B_{\rm ac}}{2}\tilde{P}_x - \frac{t}{T^2}\tilde{P}_z. \quad (24)$$

## III. LINEAR RESPONSE

In practical applications, precise measurement of weak magnetic fields is often of great interest, such as those associated with precision medicine, deep-sea exploration, cardiac activity, etc. [27]. When $B_{\rm ac}$ is weak enough, we can ignore the first term in Eq. (24). In this case, the time evolution of $\tilde{P}_z$ is decoupled with $\tilde{P}_x$, $\tilde{P}_y$, and $B_{\rm ac}$, and $\tilde{P}_x$ exhibits a linear dependence on $B_{\rm ac}$. Under the weak-field approximation, Eqs. (22)–(24) can be simplified as

$$\dot{\tilde{P}}_x = \frac{\gamma_n B_{\rm ac}}{2}\tilde{P}_z + \Delta\tilde{P}_y - \frac{t}{T^2}\tilde{P}_x, \quad (25)$$

$$\dot{\tilde{P}}_y = -\Delta\tilde{P}_x - \frac{t}{T^2}\tilde{P}_y, \quad (26)$$

$$\dot{\tilde{P}}_z = -\frac{t}{T^2}\tilde{P}_z. \quad (27)$$

When the polarization is initially along the $z$-axis, i.e., $\mathbf{P}(t=0) = (0, 0, P_0)$, the solutions to the above equations can be expressed as follows:

$$\tilde{P}_x = \frac{P_0 B_{\rm ac}\gamma_n}{2\Delta} e^{-\frac{t^2}{2T^2}}\sin(\Delta t), \quad (28)$$

$$\tilde{P}_y = \frac{P_0 B_{\rm ac}\gamma_n}{2\Delta} e^{-\frac{t^2}{2T^2}}[\cos(\Delta t) - 1], \quad (29)$$

$$\tilde{P}_z = P_0 e^{-\frac{t^2}{2T^2}}. \quad (30)$$

Since the relation between the polarization in the rotating frame and the laboratory frame is

$$P_x(t) = \tilde{P}_x(t)\cos(\omega t) - \tilde{P}_y(t)\sin(\omega t), \quad (31)$$

$$P_y(t) = \tilde{P}_x(t)\sin(\omega t) + \tilde{P}_y(t)\cos(\omega t), \quad (32)$$

$$P_z(t) = \tilde{P}_z(t), \quad (33)$$

we can obtain the polarization in the laboratory frame as

$$P_x = \frac{P_0 B_{\rm ac}\gamma_n}{2\Delta} e^{-\frac{t^2}{2T^2}}[\sin(\Delta t - \omega t) + \sin(\omega t)], \quad (34)$$

$$P_y = \frac{P_0 B_{\rm ac}\gamma_n}{2\Delta} e^{-\frac{t^2}{2T^2}}[\cos(\Delta t - \omega t) - \cos(\omega t)], \quad (35)$$

$$P_z = P_0 e^{-\frac{t^2}{2T^2}}. \quad (36)$$

Thus, the magnitude of the transverse polarization can be expressed as

$$P_\perp = \frac{P_0 B_{\rm ac}\gamma_n}{\Delta} e^{-\frac{t^2}{2T^2}} \sin\left(\frac{\Delta t}{2}\right). \tag{37}$$

According to $B_{\rm eff} = 8\pi\kappa_0 M_0 P_\perp/3$, where $\kappa_0 = 540$ denotes the Fermi-contact enhancement factor between $^{129}$Xe and $^{87}$Rb [27,54], the amplitude of the transverse effective field is

$$B_{\rm eff} = \frac{8\pi}{3}\kappa_0 M_0 \frac{P_0 B_{\rm ac}\gamma_n}{\Delta} e^{-\frac{t^2}{2T^2}} \sin\left(\frac{\Delta t}{2}\right). \tag{38}$$

Thus the transverse field is amplified by a factor

$$\Pi \equiv \frac{|\mathbf{B}_{\rm eff}|}{|\mathbf{B}_{\rm ac}|} = \frac{2\lambda M_n \gamma_n}{\Delta} \sin\left(\frac{\Delta t}{2}\right) \mathrm{e}^{-\frac{t^2}{2T^2}}, \tag{39}$$

where $M_n = M_0 P_0$ is the nuclear magnetization of $^{129}$Xe, $\lambda = 4\pi\kappa_0/3$. The optimal time $t_{\rm opt}$ can be obtained by calculating $\partial\Pi/\partial t|_{t=t_{\rm opt}} = 0$, and thus yields $\tan(\Delta t_{\rm opt}/2) = \Delta T^2/2t_{\rm opt}$. Now we expand $\tan(\Delta t_{\rm opt}/2)$ to the third order of $\Delta t_{\rm opt}$ and obtain the following expression: $(\Delta t_{\rm opt}/2)+(\Delta t_{\rm opt}/2)^3/3=\Delta T^2/2t_{\rm opt}$. The time required to reach the maximum transverse polarization is determined by

$$t_{\rm opt} = \sqrt{\frac{6}{\Delta^2}\left(-1+\sqrt{1+\frac{1}{3}\Delta^2 T^2}\right)}. \tag{40}$$

Again by Taylor expansion, we can obtain

$$t_{\rm opt} \simeq T\left(1-\frac{\Delta^2 T^2}{24}\right). \tag{41}$$

Based on this finding, it is shown that the optimal time becomes longer as $T$ increases and $\Delta$ decreases, which will be discussed in detail in the next section.

When the oscillation frequency of the external magnetic field matches the $^{129}$Xe Larmor frequency, i.e., $\Delta = 0$, the time required to reach the maximum transverse polarization is $t_{\rm opt} = T$. It should be noted that the optimal time should be smaller than $T$ in the nonresonance case, i.e., $\Delta \neq 0$. The optimal amplification factors for the Markovian and QZE cases are $\Pi = 2\lambda M_n\gamma_n T\mathrm{e}^{-1}$ [27] and $\Pi = 2\lambda M_n\gamma_n T\mathrm{e}^{-1/2}$, respectively. Therefore, the QZE can enhance the amplification of the weak magnetic field by a factor $\sqrt{\mathrm{e}}$.

## IV. NONLINEAR RESPONSE

In the following, we obtain the response of the $^{129}$Xe spins without the weak-field approximation but by solving Eqs. (22)–(24) numerically. Figure 1 shows $P_\perp$ against time in the QZE and Markovian cases [27], respectively. In order to verify the validity of the weak-field approximation, we compare the linear response with the nonlinear response under different amplitudes of the magnetic field. The approximated and the exact profiles almost overlap each other when the measured field is 10 pT. However, as the magnetic field increases, their difference becomes larger and larger, which suggests that the approximation works well in the case of weak fields. Most importantly, it is clearly observed that the response under the Gaussian noise is significantly larger than that under the Markovian noise, indicating more effective magnetic-field amplification via the QZE.

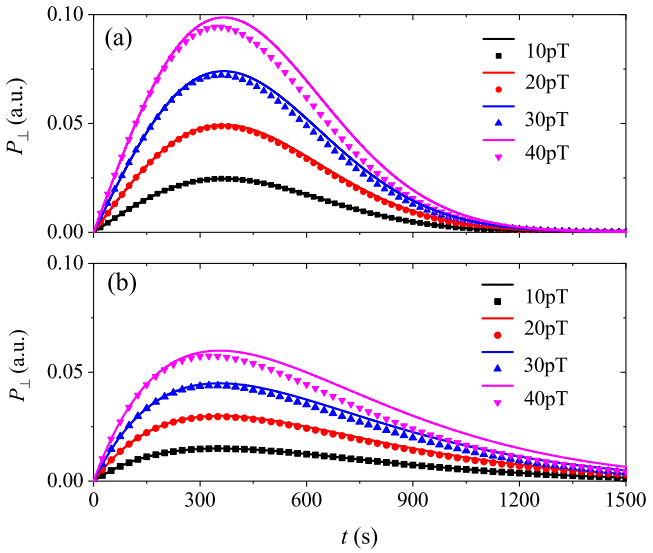


FIG. 1. Time evolution of the transverse polarization $P_\perp$ vs $B_{\rm ac}$ for (a) the Gaussian and (b) the Markovian noise, respectively. Solid lines represent the profiles under the linear-response approximation while symbols represent the profiles by the numerically exact solution. The parameters $T = 380$ s and $\Delta = 2.5$ mHz are used.

Figure 2 compares the optimal response $P_\perp^{\rm opt}$ in the Markovian case and QZE regime over a wide range of coherence times. It is shown that the optimal responses in both cases exhibit the same trend, gradually increasing with $T$. Furthermore, the response increases with the magnitude of the magnetic field for a given coherence time $T$. Interestingly, it is evident that the responses in the QZE consistently exceed those in the Markovian case.

To evaluate the effect of detuning ($\Delta$) on the amplification of the magnetic field under the QZE versus the Markovian regime, we numerically compare the optimal responses for different $B_{\rm ac}$'s. This comparison is achieved by solving the QZE dynamics Eqs. (22)–(24) in Fig. 3(a) and the Markovian dynamics Eqs. (10)–(12) in Fig. 3(b) separately. As illustrated in both Figs. 3(a) and 3(b), the optimal response decreases monotonically with increasing absolute value of detuning for a fixed value of $B_{\rm ac}$. Therefore, in order to achieve a larger amplification of the weak magnetic field, the resonance between the driving field and Larmor frequency is

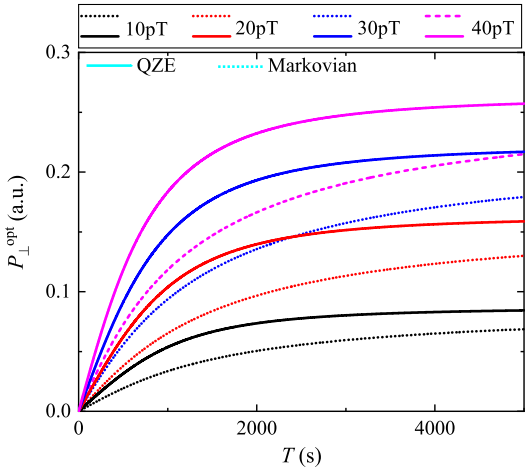


FIG. 2. The optimal transverse polarization $P_\perp^{\rm opt}$ as a function of the coherence time $T$ for different values of $B_{\rm ac}$ is presented for both Markovian dynamics (dotted lines) and the QZE (solid lines), respectively. The other parameters are the same as those used in Fig. 1.

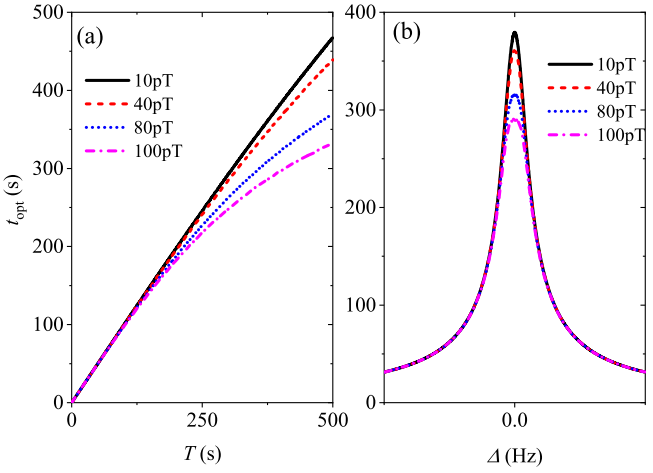


FIG. 4. Dependence of the optimal time $t_{\rm opt}$ on (a) the relaxation time $T$ with $\Delta = 2.5$ mHz and (b) the detuning $\Delta$ with $T = 380$ s for the QZE in different $B_{\rm ac}$'s.

required. Furthermore, the optimal response shows a gradual increase as the magnetic-field strength is enhanced for a constant detuning. It is obvious that the optimal responses are always smaller than the counterparts in the QZE for all $B_{\rm ac}$'s.

In Fig. 4, we present the optimal time $t_{\rm opt}$ to perform the measurement as a function of the relaxation time $T$ and detuning $\Delta$ for the QZE, respectively. It is demonstrated that $t_{\rm opt}$ is proportional to $T$ for $B_{\rm ac} = 10$ pT, which is consistent with Eq. (41). However, as $B_{\rm ac}$ increases, the time required to achieve the optimal response decreases for a given $T$. On the other hand, when talking about the dependence of the optimal measurement time on $\Delta$, it turns out to be very complicated. It requires the longest time to achieve the optimal response for the resonance case, while $t_{\rm opt}$ decreases as the detuning is enlarged, which is predicted by Eq. (41). Notably, for different magnetic fields, all curves coincide with each other in the large-detuning limit. These findings suggest that maximizing the relaxation time while minimizing the detuning is crucial for expediting the amplification of the weak magnetic field. Thus, careful control of these parameters is essential to enhance the efficiency and precision of the measurement process.

Since in Fig. 3(a), the optimal responses increase as the magnetic field is enlarged, it may be quite natural to ask whether there exists a bound for the optimal response. As depicted in Fig. 5, we explore the optimal response for different sets of $(B_{\rm ac}, \Delta)$. When the system is at resonance, the optimal response will quickly be saturated as the magnetic field is enlarged. As the absolute value of detuning increases, the smallest magnetic field to saturate the optimal response becomes lager and larger.

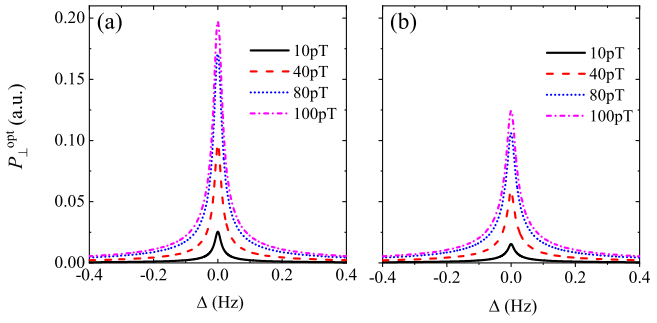


FIG. 3. The optimal transverse polarization $P_\perp^{\rm opt}$ in (a) the Gaussian noise and (b) the Markovian cases as a function of the detuning $\Delta$ for different $B_{\rm ac}$'s. The other parameters are the same as those used in Fig. 1.

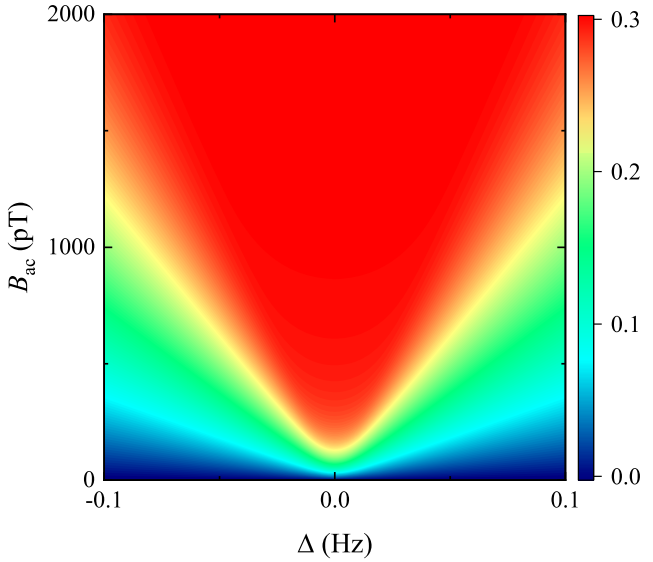


FIG. 5. Phase diagram of the optimal response $P_\perp^{\rm opt}$ vs $B_{\rm ac}$ and $\Delta$ for $T = 380$ s.

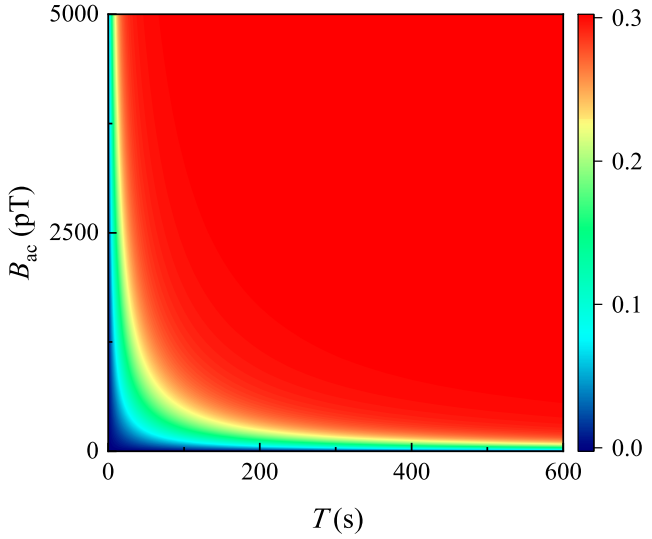


FIG. 6. Phase diagram of the optimal response $P_{\perp}^{\mathrm{opt}}$ vs $B_{\mathrm{ac}}$ and $T$ for $\Delta = 2.5$ mHz.

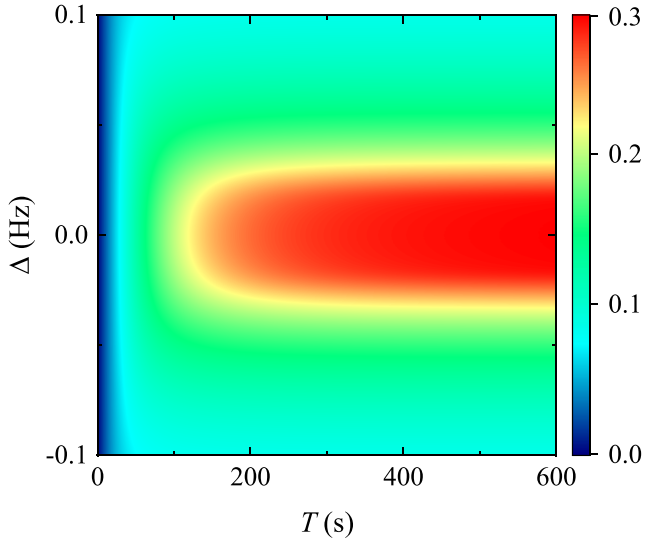


FIG. 7. Phase diagram of the optimal response $P_{\perp}^{\mathrm{opt}}$ vs $\Delta$ and $T$ for $B_{\mathrm{ac}} = 400$ pT. The other parameters are the same as those in Fig. 1.

To gain further insight into the effects of the amplitude of the oscillating field $B_{\mathrm{ac}}$ and the relaxation time $T$ on the optimal response $P_{\perp}^{\mathrm{opt}}$, we focus on the near-resonance case and present the phase diagram of the optimal response for a large range of $T$ and $B_{\mathrm{ac}}$ in Fig. 6. It is shown that the optimal response can be achieved across the majority of the parameter space $(B_{\mathrm{ac}}, T)$, which provides convenience for measuring magnetic fields of various amplitudes. However, it should be pointed out that the relaxation time $T$ should be sufficiently large, e.g., $T > 60$ s, in order to attain the maximum optimal response larger than 0.28.

On the other hand, the realistic noble-gas coherence time is much shorter than its intrinsic coherence time because of the presence of the magnetic-field gradient in experiments [27]. There are several sources of the magnetic-field gradient, including the inhomogeneity of the light intensity of the pump beam, the edge of the vapor cell that is not illuminated, the effective magnetic-field gradient from Rb polarization, and the real magnetic-field gradient from the applied bias field [27,51]. Therefore, we should try to avoid the influence of these factors on the coherence time as much as possible.

In Fig. 7, we explore the optimal response in the parameter space $(\Delta, T)$ for $B_{\mathrm{ac}} = 400$ pT. The results indicate that the optimal response is confined to a narrow parameter region characterized by a large relaxation time $T$ and a small detuning $\Delta$, as depicted by the red region.

Another application of the QZE lies in the investigation of a broad range of exotic interactions using such a quantum spin amplifier, which is introduced to resonantly amplify the effect of the exotic field $\mathbf{B}_{ac}$. $^{87}$Rb and $^{129}$Xe are polarized in both the spin-sensor cell and spin-source cell. The nuclear spins between two cells can generate an exotic spin-dependent interaction mediated by axions. The fractional composition of the $^{129}$Xe nuclear spin arising from neutrons (n) and protons (p) is 0.73 and 0.27, respectively [55]. According to Refs. [56–59], the interaction between the polarized neutrons is

$$V_{\mathrm{ps-ps}} = -\frac{g_{\mathrm{ps}}^n g_{\mathrm{ps}}^n}{16\pi m_n m_n}\left[\hat{\boldsymbol{\sigma}}_{\mathrm{so}}\cdot\hat{\boldsymbol{\sigma}}_{\mathrm{se}}\left(\frac{m_a}{r^2}+\frac{1}{r^3}\right) -(\hat{\boldsymbol{\sigma}}_{\mathrm{so}}\cdot\hat{r})(\hat{\boldsymbol{\sigma}}_{\mathrm{se}}\cdot\hat{r})\left(\frac{m_a^2}{r}+\frac{3m_a}{r^2}+\frac{3}{r^3}\right)\right]\mathrm{e}^{-m_a r}, \quad (42)$$

where $\hbar = c = 1$, $g_{\mathrm{ps}}^n$ is the pseudoscalar coupling constant of the neutron, $m_{\mathrm{n}}$ ($m_{\mathrm{a}}$) is the mass of the neutron (axion), $\hat{\boldsymbol{\sigma}}_{\mathrm{so}}$ ($\hat{\boldsymbol{\sigma}}_{\mathrm{se}}$) is the spin operator in the source (sensor) cell, and $\vec{r} = r\hat{r}$ is the distance vector between two interacting neutrons. Because of the energy shift of the nuclear spins in the spin sensor caused by such exotic interaction, the pseudomagnetic field $\mathbf{B}_{\mathrm{ac}}\hat{\boldsymbol{\sigma}}_{\mathrm{so}} = -V_{\mathrm{ps-ps}}/\nu_{\mathrm{Xe}}$ is experienced by the nuclear spins in the sensor cell, where $\nu_{\mathrm{Xe}}$ is the magnetic moment of the nuclear spin in the sensor cell, and

$$B_{\mathrm{ac}}(\mathbf{r}) = \frac{g_{\mathrm{ps}}^n g_{\mathrm{ps}}^n}{16\pi m_n m_n \nu_{\mathrm{Xe}}}\left[\hat{\sigma}_{\mathrm{II}}\left(\frac{1}{\lambda r^2}+\frac{1}{r^3}\right) - \hat{r}(\hat{\sigma}_{\mathrm{II}}\cdot\hat{r}) \times\left(\frac{1}{\lambda^2 r}+\frac{3}{\lambda r^2}+\frac{3}{r^3}\right)\right]e^{-r/\lambda}, \quad (43)$$

where $\lambda$ is the Compton wavelength. It is useful to set a new constraint $|g_{\mathrm{ps}}^n g_{\mathrm{ps}}^n|$ by searching for interactions $V_{\mathrm{ps-ps}}$. Consequently, $^{129}$Xe constitutes a natural advantage in searches for neutron spin-dependent couplings.

Figure 8 shows the obtained constraints on $|g_{\mathrm{ps}}^n g_{\mathrm{ps}}^n|/4$ set by this work together with the limits from the previous experimental searches [26,51,60,61]. The excluded values of the coupling-constants product of the previous results are presented as the light-gray areas and the result of this work

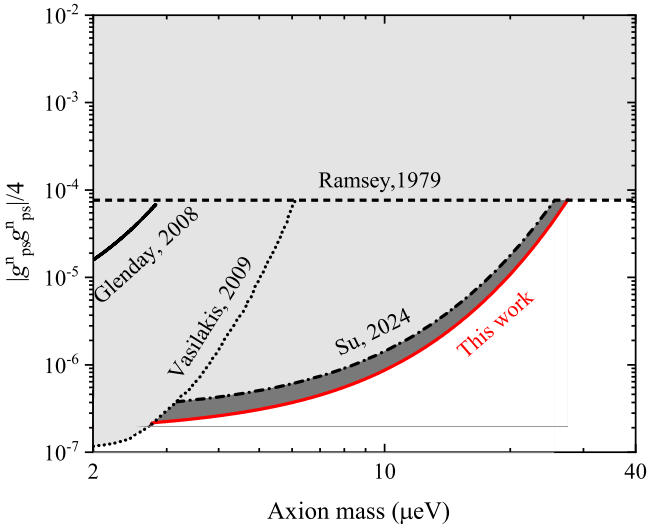


FIG. 8. Constraints to the coupling-constants product $|g^n_{ps}g^n_{ps}|/4$ within the axion window. The black curves represent the constraints on exotic interactions between protons from the previous experiments of Ramsey [61], Glenday *et al.* [60], Vasilakis *et al.* [26], and Su *et al.* [51] as a function of the axion mass. The red line represents the new constraints on axions or ALPs obtained from our theory, which establishes an improved bound by a factor about $e^{1/2}$ due to the QZE.

is presented as the dark-gray area. The first constraint of exotic spin-spin interactions was derived by Ramsey [61] and presented as the black dashed line. The black solid and dotted lines respectively represent the constraints on $|g^n_{ps}g^n_{ps}|/4$ placed by the maser [60] and the comagnetometer [26] experiments. The black dashed-dotted line represents the laboratory constraints on $|g^n_{ps}g^n_{ps}|/4$ placed by the $^{129}$Xe magnetometer [51]. As mentioned above, we enhance the amplification of the weak magnetic field by a factor $e^{1/2}$ based on their work. Accordingly, we effectively estimate the most stringent constraint on $|g^n_{ps}g^n_{ps}|/4$ by utilizing the QZE from a theoretical perspective and present it as the red solid line, part of which reaches into the unexplored parameter space within the axion window. For the mass range from 3.2 to 24.3 μeV, we improve the previous constraint on neutron-neutron spin coupling by a factor about $e^{1/2}$ for the mass range from 3.2 to 24.3 μeV. The major improvement in the constraint comes from the QZE. In addition, our theoretical approach can also be utilized to search for other exotic spin-dependent interactions, such as those between the polarized electrons, and between a polarized electron and an unpolarized nucleon. Since it has not yet been implemented in the experiments, we not only provide the optimal measurement parameters but also obtain optimal amplification, i.e., about 8900, and the corresponding time for the practical experiments, which can effectively guide a related experiment in this work. We hope that the experiment can be realized in this overlapping spin ensemble by the QZE in the near future, contributing to the detection of exotic interactions and ALPs.

## V. CONCLUSION

In this paper, we propose a noble-gas spin evolution in the dark and amplify the measurement of the weak magnetic field by the QZE. Recently, there has been significant progress in amplifying the weak magnetic field with mixtures of nuclear-spin-polarized noble gases and vapors of spin-polarized alkali-metal atoms, such as $^{129}$Xe – $^{87}$Rb [5,27,62]. This technique can also be applied to various alkali-metal atoms and noble gases, including K-$^{129}$Xe, K-$^{3}$He, $^{87}$Rb – $^{21}$Ne, etc. In experiments, $^{129}$Xe gas overlapping $^{87}$Rb gas can be used in the same vapor cell, wherein the atomic system is inherently subjected to the Gaussian noise in the short-time regime. It can be interpreted from a quantum-mechanical perspective; i.e., the dynamics of an arbitrary open quantum system begins with a Gaussian decay, and transitions to Markovian dynamics, and ultimately ends in a power-law decay in the long-time regime [63,64]. The short-time domain has long attracted considerable attention due to its role in generating the QZE under specific physical conditions. Nevertheless, the Zeno dynamics is commonly ignored, owing to its behavior on short timescales in such atomic systems. For example, the free-induction-decay signal of polarized $^{3}$He reported in Ref. [65] clearly exhibits a Gaussian-type decay characterized by the Zeno dynamics. Actually, the QZE is not limited to open quantum systems but extends universally to closed quantum systems, representing an intrinsic quantum manifestation arising from the unitarity of quantum evolution. If the QZE is applied to this technique, this kind of experiment will be enhanced with a more-significant magnetic-field amplification effect. Thus it can be used to search for axions, dark photons, axion-mediated spin-dependent interactions, etc. Since the results of this work provide more significant magnetic amplification, we hope that our studies will stimulate experiments on establishing new constraints of dark matter and exotic interactions by this method.

In summary, we exploit the magnetic amplification considering the QZE through effective fields from collisions between alkali-metal atoms and noble-gas atoms, increasing the magnetic magnification by up to about 1.65-fold relative to the Markovian noise. Based on our analysis, we obtain the optimal time required to reach the maximum transverse polarization and thus the optimal response under different combinations of the parameters. Our results indicate that the amplification of measuring the weak fields can be further enhanced by the QZE as compared to the Markovian case. This indicates that our research can further improve the accuracy of weak-field measurements.

## ACKNOWLEDGMENTS

We are grateful to Hai-Yang Yan and Gu-Zhi Bao for their valuable suggestions and discussions. This work is supported by Quantum Science and Technology-National Science and Technology Major Project (2023ZD0300200), and the

National Natural Science Foundation of China under Grant No. 62461160263.

## DATA AVAILABILITY

The data are not publicly available. The data are available from the authors upon reasonable request.

## APPENDIX A: DYNAMICS IN NON-MARKOVIAN ENVIRONMENTS

In this section, we provide the dynamics of the transverse polarization theoretically as follows. Taking the interaction of the system with the environment into account, the $^{129}$Xe nuclear spin in a magnetic field is described by the following Hamiltonian:

$$\hat{H} = \hat{H}_S + \hat{H}_{SB}, \tag{A1}$$

where

$$\hat{H}_S = -\gamma_n B_0 \hat{I}_z - \gamma_n B_{\rm ac}\cos(2\pi\nu t)\hat{I}_y, \tag{A2}$$

$$\hat{H}_{SB} = \sum_k \omega_k a_k^\dagger a_k + \sum_k g_k I_x (a_k + a_k^\dagger), \tag{A3}$$

where $B_0$ and $B_{ac}$ are the experienced field by $^{129}$Xe nuclear spins along the $Z$-axis and $Y$-axis respectively with $\nu$ being the Larmor frequency of the nuclear spins in the source cell. For the resonance case, in the rotating frame the spin Hamiltonian with the total field reads explicitly

$$\hat{\tilde{H}} = -\frac{\gamma_n B_{\rm ac}}{2}\hat{I}'_z + \sum_k (\omega_k - 2\pi\nu)\hat{a}_k^\dagger \hat{a}_k + \sum_k g_k(\hat{I}'_+ \hat{a}_k + \hat{I}'_- \hat{a}_k^\dagger). \tag{A4}$$

In the subspace of single and zero excitation, we assume that the wave function is

$$|\psi(t)\rangle = \alpha(t)|0,e\rangle + \sum_k \beta_k(t)|k,g\rangle + \gamma|g,0\rangle. \tag{A5}$$

Inserting Eqs. (A4) and (A5) into the Schrödinger equation $id|\psi(t)\rangle/dt = H|\psi(t)\rangle$, we can obtain

$$\dot{\alpha}(t) - i\frac{\gamma_n B_{\rm ac}}{2}\alpha(t) + \sum_k g_k \beta_k(t) = 0, \tag{A6}$$

$$\dot{\beta}_k(t) + i\left(\frac{\gamma_n B_{\rm ac}}{2} + \omega - 2\pi\nu\right)\beta_k(t) - g_k\alpha(t) = 0. \tag{A7}$$

We can calculate $\alpha(t) = c(t)\alpha(0) + \sum_k d_k(t)\beta_k(0)$ under the initial conditions $c(0) = 1, d_k(0) = 0$, where $c(t)$ is determined by

$$\dot{c}(t) - i\frac{\gamma_n B_{\rm ac}}{2}c(t) - \int_0^t f(t-\tau)c(\tau)d\tau = 0. \tag{A8}$$

Then, if we take the Markovian approximation to have $c'(\tau) \simeq c'(t)$ and replace $\int_0^t d\tau$ by $\int_0^\infty d\tau$, we can obtain

$$c(t) = e^{[i(\frac{\gamma B_{ac}}{2} - \Delta) - \kappa]t}, \tag{A9}$$

where $\Delta = \mathcal{P}\int_0^\infty J(\omega)/(\gamma B_{ac} + \omega - 2\pi\nu)d\omega$ is the Lamb shift due to the bath, $\kappa = \pi J(2\pi\nu - \gamma B_{ac})$. The coupling is characterized by the Lorentzian spectral density $J(\omega) = ag/\pi(g^2 + \omega^2)$, where $a > 0$ regulates the coupling strength. However, if we only take the half Markovian approximation to have $c'(\tau) \simeq c'(t)$, we can obtain

$$c(t) = e^{i(\frac{\gamma B_{ac}}{2} - \Delta)t - \gamma(t)}, \tag{A10}$$

where [36]

$$\gamma(t) = \frac{a}{4g}\left[\frac{1}{g}(e^{-gt} - 1) + t\right] \tag{A11}$$

for $t \geq 0$ and $g \geq 0$. In the short-time regime, i.e., $gt \ll 1$, we have

$$\gamma(t) \simeq \frac{a}{8}t^2. \tag{A12}$$

Thus, the Zeno time reads

$$T_Z = \sqrt{\frac{8}{a}}. \tag{A13}$$

In the long-time regime, i.e., $gt \gg 1$, we have

$$\gamma(t) \approx \frac{at}{4g}. \tag{A14}$$

Thus, the Markovian time reads

$$T_M = \frac{4g}{a}. \tag{A15}$$

The relationship between $T_M$ and $T_Z$ is expressed as

$$T_Z = \frac{\sqrt{2a}}{2g}T_M. \tag{A16}$$

For a fixed pair of $a$ and $g$, $T_Z$ is proportional to $T_M$. In other words, we can prolong $T_Z$ when $T_M$ is prolonged.

## APPENDIX B: QUANTITATIVE ESTIMATION OF THE RELAXATION TIME

The traverse relaxation time of spin-polarized noble gas can be expressed as

$$\frac{1}{T_2} = \frac{8\gamma^2 R^4 |\nabla B_z|^2}{175D} + \frac{1}{2T_1} \tag{B1}$$

in the spherical cell of radius $R$ subjected to a gradient along the $z$-axis [66], where $|\nabla B_z|^2$ is the bias magnetic-field gradient along the $z$-axis, and $D$ is the diffusion constant of noble gas atoms in the atomic cell. In Ref. [27], the Rb polarization-induced effective magnetic-field gradient is greatly suppressed when the Rb pump light is off, resulting in the effect of the magnetic-field gradient being ignored. Thus, we assume $1/T_2 \approx 1/2T_1$ at first. The relaxation rate of noble gas $1/T_1$ can be expressed as [67–72]

$$\frac{1}{T_1} = \frac{1}{T_1^{\nabla}} + \frac{1}{T_1^{\text{wall}}} + \frac{1}{T_1^{\text{d-d}}}, \tag{B2}$$

where $1/T_1^{\nabla}$ represents the relaxation rate due to the magnetic-field inhomogeneity, and $1/T_1^{\text{wall}}$ which arises from interaction with the container surface, is typically observed to be proportional to the surface-to-volume ratio [68], i.e., $1/T_1^{\text{wall}} = \eta S/V$. In glass vessels, $T_1^{\text{wall}}$ has been successfully increased to above 100 h [73]. Consequently, the second term of Eq. (B2) can be neglected. $1/T_1^{\text{d-d}}$ arises from the magnetic dipole-dipole interaction associated with binary atomic collisions, i.e., $1/T_1^{\text{d-d}} = (3600)^{-1} n/817 n_0$ [73]. Under standard conditions with the noble-gas pressure being 1 bar, we have $n = n_0 = 2.687 \times 10^{25}$. $1/T_1^{\nabla}$ can be expressed as [74,75]

$$\frac{1}{T_1^{\nabla}} = \frac{0.14\sqrt{T}}{P_r B_0^2}(|\nabla B_x|^2 + |\nabla B_y|^2), \tag{B3}$$

where $T$ is the temperature within the gas cell, and $P_r$ represents the pressure of noble gas in bars. This pressure can be expressed as $P_r = nk_B T$, where $n$ is the particle-number density of the noble gas in bars, and $k_B$ is the Boltzmann constant. $\nabla B_x$ and $\nabla B_y$ are the gradients in the transverse components of the magnetic field. The expression for $T_2$ is simplified as

$$\frac{1}{T_2} \approx \frac{0.07}{nk_B\sqrt{T}B_0^2}(|\nabla B_x|^2 + |\nabla B_y|^2). \tag{B4}$$

The Zeno time was found to be 170 ms in the experiment [65]. To achieve a Zeno time on the order of $10^2$ s, the transverse relaxation time $T_2$ should also be increased to the order of $10^2$ s according to Eq. (A16). If $B_0$ is increased by a factor of 10, and the temperature $T$ is raised by 2 times, and the particle-number density $n$ is enhanced by 5 times, and the magnetic-field gradient is reduced by a half, the value of $T_2$ can be enhanced by a factor of 2830. At present, we can obtain $T_1^{\text{d-d}} \approx 1.45 \times 10^7$ s and $T_1^{\nabla} \approx 2600$ s, and we also find that the conditions $T_1^{\text{wall}} \gg T_1^{\nabla}$ and $T_1^{\text{d-d}} \gg T_1^{\nabla}$ are satisfied. Therefore, the second and third terms of Eq. (B2) are also negligible. According to Eq. (A16), the Zeno time $T_Z$ can be enhanced from 170 ms to 480 s, and then the Zeno dynamics could be observed with current experimental setups.


[1] D. N. Spergel, The dark side of cosmology: Dark matter and dark energy, Science **347**, 1100 (2015).
[2] G. Bertone and D. Hooper, History of dark matter, Rev. Mod. Phys. **90**, 045002 (2018).
[3] P. Sikivie, Invisible axion search methods, Rev. Mod. Phys. **93**, 015004 (2021).
[4] Y. M. Andreev *et al.* (NA64 Collaboration), Search for a new $B - L$ $Z'$ gauge boson with the NA64 experiment at CERN, Phys. Rev. Lett. **129**, 161801 (2022).
[5] H. Su, Y. Wang, M. Jiang, W. Ji, P. Fadeev, D. Hu, X. Peng, and D. Budker, Search for exotic spin-dependent interactions with a spin-based amplifier, Sci. Adv. **7**, eabi9535 (2021).
[6] Y. Hochberg, I. Charaev, S.-W. Nam, V. Verma, M. Colangelo, and K. K. Berggren, Detecting sub-GeV dark matter with superconducting nanowires, Phys. Rev. Lett. **123**, 151802 (2019).
[7] J. Manley, M. D. Chowdhury, D. Grin, S. Singh, and D. J. Wilson, Searching for vector dark matter with an optomechanical accelerometer, Phys. Rev. Lett. **126**, 061301 (2021).
[8] D. DeMille, J. M. Doyle, and A. O. Sushkov, Probing the frontiers of particle physics with tabletop-scale experiments, Science **357**, 990 (2017).
[9] M. S. Safronova, D. Budker, D. DeMille, D. F. J. Kimball, A. Derevianko, and C. W. Clark, Search for new physics with atoms and molecules, Rev. Mod. Phys. **90**, 025008 (2018).
[10] R. Bradley, J. Clarke, D. Kinion, L. J. Rosenberg, K. van Bibber, S. Matsuki, M. Mück, and P. Sikivie, Microwave cavity searches for dark-matter axions, Rev. Mod. Phys. **75**, 777 (2003).
[11] V. Anastassopoulos *et al.* (C. A. S. T. Collaboration), New cast limit on the axion–photon interaction, Nat. Phys. **13**, 584 (2017).
[12] T. Braine *et al.* (ADMX Collaboration), Extended search for the invisible axion with the axion dark matter experiment, Phys. Rev. Lett. **124**, 101303 (2020).
[13] J. L. Ouellet, C. P. Salemi, J. W. Foster, R. Henning, Z. Bogorad, J. M. Conrad, J. A. Formaggio, Y. Kahn, J. Minervini, A. Radovinsky, N. L. Rodd, B. R. Safdi, J. Thaler, D. Winklehner, and L. Winslow, First results from

abracadabra-10 cm: A search for sub-μeV axion dark matter, Phys. Rev. Lett. **122**, 121802 (2019).
[14] M. Jiang, H. Su, Z. Wu, X. Peng, and D. Budker, Floquet maser, Sci. Adv. **7**, eabe0719 (2021).
[15] D. W. P. Amaral, D. G. Uitenbroek, T. H. Oosterkamp, and C. D. Tunnell, First search for ultralight dark matter using a magnetically levitated particle, Phys. Rev. Lett. **134**, 251001 (2025).
[16] S. Kotler, N. Akerman, Y. Glickman, A. Keselman, and R. Ozeri, Single-ion quantum lock-in amplifier, Nature (London) **473**, 61 (2011).
[17] S. C. Burd, R. Srinivas, J. J. Bollinger, A. C. Wilson, D. J. Wineland, D. Leibfried, D. H. Slichter, and D. T. C. Allcock, Quantum amplification of mechanical oscillator motion, Science **364**, 1163 (2019).
[18] M. Jiang, Y. Qin, X. Wang, Y. Wang, H. Su, X. Peng, and D. Budker, Floquet spin amplification, Phys. Rev. Lett. **128**, 233201 (2022).
[19] M. Schaffry, E. M. Gauger, J. J. L. Morton, and S. C. Benjamin, Proposed spin amplification for magnetic sensors employing crystal defects, Phys. Rev. Lett. **107**, 207210 (2011).
[20] A. Zavatta, J. Fiurášek, and M. Bellini, A high-fidelity noiseless amplifier for quantum light states, Nat. Photonics **5**, 52 (2011).
[21] S. Afach *et al.*, Search for topological defect dark matter with a global network of optical magnetometers, Nat. Phys. **17**, 1396 (2021).
[22] C. Dailey, C. Bradley, J. D. Kimball, I. Sulai, S. Pustelny, A. Wickenbrock, and A. Derevianko, Quantum sensor networks as exotic field telescopes for multi-messenger astronomy, Nat. Astron. **5**, 150 (2021).
[23] J. Chang, R. Essig, and S. McDermott, Supernova 1987A constraints on sub-GeV dark sectors, millicharged particles, the QCD axion, and an axion-like particle, J. High Energy Phys. 09 (2018) 051.
[24] A. Almasi, J. Lee, H. Winarto, M. Smiciklas, and M. Romalis, New limits on anomalous spin-spin interactions, Phys. Rev. Lett. **125**, 201802 (2020).
[25] J. Lee, A. Almasi, and M. Romalis, Improved limits on spin-mass interactions, Phys. Rev. Lett. **120**, 161801 (2018).
[26] G. Vasilakis, J. M. Brown, T. W. Kornack, and M. V. Romalis, Limits on new long range nuclear spin-dependent forces set with a K-$^3$He comagnetometer, Phys. Rev. Lett. **103**, 261801 (2009).
[27] M. Jiang, Y. Huang, C. Guo, H. Su, Y. Wang, X. Peng, and D. Budker, Observation of magnetic amplification using dark spins, Proc. Natl. Acad. Sci. U.S.A. **121**, e2315696121 (2024).
[28] B. Misra and E. C. G. Sudarshan, The Zeno's paradox in quantum theory, J. Math. Phys. (N.Y.) **18**, 756 (1977).
[29] A. Peres and A. Ron, Incomplete "collapse" and partial quantum Zeno effect, Phys. Rev. A **42**, 5720 (1990).
[30] E. Block and P. R. Berman, Quantum Zeno effect and quantum Zeno paradox in atomic physics, Phys. Rev. A **44**, 1466 (1991).
[31] Q. Ai, Y. Li, H. Zheng, and C. P. Sun, Quantum anti-Zeno effect without rotating wave approximation, Phys. Rev. A **81**, 042116 (2010).
[32] D. Z. Xu, Q. Ai, and C. P. Sun, Dispersive-coupling-based quantum Zeno effect in a cavity-QED system, Phys. Rev. A **83**, 022107 (2011).
[33] J. Zhang, J. Jing, L. Wang, and S. Zhu, Criterion for quantum Zeno and anti-Zeno effects, Phys. Rev. A **98**, 012135 (2018).
[34] P. Facchi and S. Pascazio, Quantum Zeno dynamics: Mathematical and physical aspects, J. Phys. A **41**, 493001 (2008).
[35] L.-A. Wu, D. A. Lidar, and S. Schneider, Long-range entanglement generation via frequent measurements, Phys. Rev. A **70**, 032322 (2004).
[36] A. W. Chin, S. F. Huelga, and M. B. Plenio, Quantum metrology in non-Markovian environments, Phys. Rev. Lett. **109**, 233601 (2012).
[37] Y. Matsuzaki, S. C. Benjamin, and J. Fitzsimons, Magnetic field sensing beyond the standard quantum limit under the effect of decoherence, Phys. Rev. A **84**, 012103 (2011).
[38] X. Long, W.-T. He, N.-N. Zhang, K. Tang, Z. Lin, H. Liu, X. Nie, G. Feng, J. Li, T. Xin, Q. Ai, and D. Lu, Entanglement-enhanced quantum metrology in colored noise by quantum Zeno effect, Phys. Rev. Lett. **129**, 070502 (2022).
[39] W. Itano, D. J. Heinzen, J. J. Bollinger, and D. J. Wineland, Quantum Zeno effect, Phys. Rev. A **41**, 2295 (1990).
[40] C. Balzer, R. Huesmann, W. Neuhauser, and P. Toschek, The quantum Zeno effect-evolution of an atom impeded by measurement, Opt. Commun. **180**, 115 (2000).
[41] M. C. Fischer, B. Gutiérrez-Medina, and M. G. Raizen, Observation of the quantum Zeno and anti-Zeno effects in an unstable system, Phys. Rev. Lett. **87**, 040402 (2001).
[42] S. Wilkinson, C. Bharucha, M. Fischer, K. Madison, P. Morrow, Q. Niu, B. Sundaram, and M. Raizen, Experimental evidence for non-exponential decay in quantum tunnelling, Nature (London) **387**, 575 (1997).
[43] E. Streed, J. Mun, M. Boyd, G. Campbell, P. Medley, W. Ketterle, and D. Pritchard, Continuous and pulsed quantum Zeno effect, Phys. Rev. Lett. **97**, 260402 (2006).
[44] B. Nagels, L. J. F. Hermans, and P. L. Chapovsky, Quantum Zeno effect induced by collisions, Phys. Rev. Lett. **79**, 3097 (1997).
[45] F. Schäfer, I. Herrera, S. Cherukattil, C. Lovecchio, F. S. Cataliotti, F. Caruso, and A. Smerzi, Experimental realization of quantum Zeno dynamics, Nat. Commun. **5**, 3194 (2014).
[46] N. Kalb, J. Cramer, D. J. Twitchen, M. Markham, R. Hanson, and T. H. Taminiau, Experimental creation of quantum Zeno subspaces by repeated multi-spin projections in diamond, Nat. Commun. **7**, 13111 (2016).
[47] A. Potočnik, A. Bargerbos, F. A. Y. N. Schröder, S. A. Khan, M. C. Collodo, S. Gasparinetti, Y. Salathé, C. Creatore, C. Eichler, H. E. Türeci, A. W. Chin, and A. Wallraff, Studying light-harvesting models with superconducting circuits, Nat. Commun. **9**, 904 (2018).
[48] K. Kakuyanagi, T. Baba, Y. Matsuzaki, H. Nakano, S. Saito, and K. Semba, Observation of quantum Zeno effect in a superconducting flux qubit, New J. Phys. **17**, 063035 (2015).
[49] D. H. Slichter, C. Müller, R. Vijay, S. J. Weber, A. Blais, and I. Siddiqi, Quantum Zeno effect in the strong measurement regime of circuit quantum electrodynamics, New J. Phys. **18**, 053031 (2016).

[50] L. Bretheau, P. Campagne-Ibarcq, E. Flurin, F. Mallet, and B. Huard, Quantum dynamics of an electromagnetic mode that cannot contain $N$ photons, Science **348**, 776 (2015).
[51] H. Su, M. Jiang, Y. Wang, Y. Huang, X. Kang, W. Ji, X. Peng, and D. Budker, New constraints on axion-mediated spin interactions using magnetic amplification, Phys. Rev. Lett. **133**, 191801 (2024).
[52] M. H. Levitt, *Spin Dynamics: Basics of Nuclear Magnetic Resonance*, 2nd ed. (John Wiley & Sons, UK, 2013).
[53] H. P. Breuer and F. Petruccione, *The Theory of Open Quantum Systems* (Oxford University Press, New York, 2002).
[54] T. Walker and W. Happer, Spin-exchange optical pumping of noble-gas nuclei, Rev. Mod. Phys. **69**, 629 (1997).
[55] D. F. J. Kimball, Nuclear spin content and constraints on exotic spin-dependent couplings, New J. Phys. **17**, 073008 (2015).
[56] J. E. Moody and F. Wilczek, New macroscopic forces?, Phys. Rev. D **30**, 130 (1984).
[57] B. A. Dobrescu and I. Mocioiu, Spin-dependent macroscopic forces from new particle exchange, J. High Energy Phys. 11 (2006) 005.
[58] P. Fadeev, Y. V. Stadnik, F. Ficek, M. G. Kozlov, V. V. Flambaum, and D. Budker, Revisiting spin-dependent forces mediated by new bosons: Potentials in the coordinate-space representation for macroscopic- and atomic-scale experiments, Phys. Rev. A **99**, 022113 (2019).
[59] L. Cong, W. Ji, P. Fadeev, F. Ficek, M. Jiang, V. V. Flambaum, H. Guan, D. F. J. Kimball, M. G. Kozlov, Y. V. Stadnik, and D. Budker, Spin-dependent exotic interactions, Rev. Mod. Phys. **97**, 025005 (2025).
[60] A. G. Glenday, C. E. Cramer, D. F. Phillips, and R. L. Walsworth, Limits on anomalous spin-spin couplings between neutrons, Phys. Rev. Lett. **101**, 261801 (2008).
[61] N. F. Ramsey, The tensor force between two protons at long range, Physica A (Amsterdam) **96**, 285 (1979).
[62] M. Jiang, H. Su, A. Garcon, X. Peng, and D. Budker, Search for axion-like dark matter with spin-based amplifiers, Nat. Phys. **17**, 1402 (2021).
[63] P. Facchi, H. Nakazato, and S. Pascazio, From the quantum Zeno to the inverse quantum Zeno effect, Phys. Rev. Lett. **86**, 2699 (2001).
[64] H. Nakazato, M. Namiki, and S. Pascazio, Temporal behavior of quantum mechanical systems, Int. J. Mod. Phys. B **10**, 247 (1996).
[65] M. E. Hayden, E. Baudin, G. Tastevin, and P. J. Nacher, Nmr time reversal as a probe of incipient turbulent spin dynamics, Phys. Rev. Lett. **99**, 137602 (2007).
[66] D. D. McGregor, Transverse relaxation of spin-polarized $^3$He gas due to a magnetic field gradient, Phys. Rev. A **41**, 2631 (1990).
[67] R. S. Timsit, J. M. Daniels, and A. D. May, Nuclear relaxation of $^3$He gas on various solid surfaces, Can. J. Phys. **49**, 560 (1971).
[68] W. A. Fitzsimmons, L. L. Tankersley, and G. K. Walters, Nature of surface-induced nuclear-spin relaxation of gaseous he$^3$, Phys. Rev. **179**, 156 (1969).
[69] W. Korsch, R. Carr, D. DeSchepper, A. Dvoredsky, L. Kramer, Y. Li, R. McKeown, R. Milner, S. Pate, M. Pitt, and T. Shin, Temperature dependence of $^3$He polarization in aluminum storage cells, Nucl. Instrum. Methods Phys. Res., Sect. A **389**, 389 (1997).
[70] E. Babcock and A. Ioffe, Polarized $^3$He neutron spin filter program at the JCNS, Physica B (Amsterdam) **406**, 2448 (2011).
[71] S. Parnell, E. Babcock, K. Nünighoff, M. Skoda, S. Boag, S. Masalovich, W. Chen, R. Georgii, J. Wild, and C. Frost, Study of spin-exchange optically pumped $^3$He cells with high polarisation and long lifetimes, Nucl. Instrum. Methods Phys. Res., Sect. A **598**, 774 (2009).
[72] T. R. Gentile, P. J. Nacher, B. Saam, and T. G. Walker, Optically polarized $^3$He, Rev. Mod. Phys. **89**, 045004 (2017).
[73] W. Heil, H. Humblot, E. Otten, M. Schafer, R. Sarkau, and M. Leduc, Very long nuclear relaxation times of spin polarized helium 3 in metal coated cells, Phys. Lett. A **201**, 337 (1995).
[74] H. Y. Yan, Applications of polarized helium-3 filters in neutron scattering, Ph.D. thesis, Indiana University, 2008.
[75] J. X. Ma, Y. Lan, and H. Y. Yan, Experimental design and optimization of resonant search for exotic axion-like particles, Sci. Sin. (Engl. Ed.) **52**, 112011 (2022).